New Journal of Chemistry, Electronic Supporting Information for

A simple approach for controlled deposition of Prussian Blue Analogues nanoparticles on a functionalised plasmonic gold surface†

Giang Ngo,[a] Gautier Félix,*[a] Jérôme Long,[a] Luca Costa,[b] Oscar Saavedra V.,[b] Pierre-Emmanuel Milhiet,[b] Jean-Marie Devoisselle,[a] Yannick Guari,[a] Joulia Larionova,[a] Joël Chopineau*[a,c]

Materials

All chemical reagents were purchased and used without further purification: Potassium ferricyanide (Acros Organics, 99%), Nickel (II) chloride hexahydrate (Chimica, 99%), 2-aminoethanethiol hydrochloride (Sigma Aldrich, 98%). Ultra-pure water was obtained from a MilliQ apparatus (Millipore).

Gold coated glass slides (including 2 ± 0.5 nm thickness of chromium layer and 47 ± 1 nm thickness of gold layer) (size: 2.5 x 3.7 cm) were obtained from Femto (Besançon, France).

Synthesis of 35 nm $K^+/Ni^{2+}/[Fe(CN)_6]^{3-}$ PBA nanoparticles.

The two aqueous solutions of reactants: $NiCl_2.6H_2O$ (16 mM, 50 mL) and $K_3[Fe(CN)_6]$ (17 mM, 50 mL) were added simultaneously to 100 mL of MilliQ water using a two-syringe infusion pump (KdScientific KDS200) with a fixed addition rate at 4 $mL.min^{-1}$, under vigorous stirring at 25°C.

After completion of the addition, the solution was stirred for one hour and then centrifuged at 35700 *xg* during 10 min. The supernatant was removed and $K^+/Ni^{2+}/[Fe(CN)_6]^{3-}$ nanoparticles were recovered by centrifugation and washed with MilliQ water (3 times) and ethanol (1 time), finally dried under vacuum. In a typical experiment, about 100 mg of nanoparticles were obtained.[1, 2]

Amino coated gold surfaces

Cysteamine (aminoethane thiol) anchoring on glass was formed by immersing the gold coated glass slides overnight in an ethanol solution containing 5 mM of cysteamine hydrochloride [3]. The glass slides were thoroughly rinsed with MilliQ water and the surface was neutralised by immersing the slides in 35 mL of NaOH solution (0.1M) for 10 min. After thoroughly rinsing with water, the amino coated glass slides were dried under nitrogen flow.

In situ $K^+/Ni^{2+}/[Fe(CN)_6]^{3-}$ NPs deposition on Cysteamine-modified Gold surface (AuCyst) for Surface Plasmon Resonance measurements

Nanoparticles colloidal suspensions in MilliQ water were supplied at different concentrations: 2.50; 1.50; 0.62; 0.31; 0.16; 0.08 and 0.04 $mg.mL^{-1}$. The scheme (Fig. 1 (a)) describes the method used for assembling nanoparticles on the gold-coated glass slide using a homemade SPR PTFE cell. In this device, the glass slide was mounted on the SPR flow cell (1 mL in volume) with the amino coated layer facing the interior of the cell. After 8 hours of nanoparticles deposition, MilliQ water was injected to rinse the cell. The cell was then dried by flowing nitrogen gas. SPR measurements were performed at the air interface.

Characterization methods

Physical characterization. The hydrodynamic diameter and zeta potential of the nanoparticles were measured on a Nano ZS Zetasizer (Malvern, UK).

Transmission Electron Microscopy (TEM, JEOL 1200 EX II and LaB6 JEOL 1400 Plus) was used to determine the morphology of single PBA nanoparticles. Samples for TEM measurements were deposited from suspensions on copper grids. NPs size distribution histograms were determined using enlarged TEM micrographs taken at magnification of 100K on a statistical sample of ca. 200 NPs.

Fourrier transformed infra-red (FTIR) spectroscopy. Infrared spectra in transmission mode of nanoparticles were recorded in a dried KBr matrix formatted as disks on Spectrum Two FT-IR spectrophotometer (Spectrum 100, Perkin Elmer, US).

Attenuated total reflection (ATR)-FTIR. The deposition of PBA NPs on amino-gold, ATR-FTIR measurements were performed using attenuated total reflection accessory on a Spectrum Two FT-IR Spectrophotometer. A background without sample was acquired prior measurements.

Powder X-ray diffraction. The powder X-ray diffraction pattern (XRDP) was recorded in the interval 2θ = 10-80° at room temperature with the XPERTpro Panalytical diffractometer mounted in a Debye-Scherrer configuration and equipped with a Cu Kα radiation. The XRDP planar configuration with fixed sample and rotation diffraction angle was used.

Surface plasmon resonance (SPR) experiments and calculations. For performing SPR measurements, the SPR cell was mounted on the SPR bench. One side of the cover glass is coated with gold (inside of the cell) while the other was colligated to a right angle prism (N-BK7, 20 mm) by using an appropriate matching index oil (Invoil 704, BCP Instruments, France). Plasmon excitation was achieved via a p-polarised light from a standard 632.8 nm HeNe laser. A lock-in amplifier (including pre-amplifier and chopper) was equipped in order to maximize the signal-to-noise ratio and reject stray light. The SPR cell coupled to the prism was mounted on a precise goniometer stage for precise control of incoming and reflected light beam. The incidence angle was monitored between 38° and 50° by rotating the sample

cell and detector turntable motors with 0.05° steps. The control of the spectrometer was done via WASPLAS software. The obtained data were analysed using the generalised Rouard method and Maxwell-Garnett equation in a homemade python code, in order to determine the refractive index of NPs. For the simulation, we have taken a multi-layer system with the following composition: an infinite glass layer (to modelise the prism), a chromium layer of 2 nm, a gold layer of 47 nm, a layer of PBA NPs, an infinite layer of air. To be approximated as a homogeneous and flat layer, the NPs were considered as defect in a matrix (in our case the air). The height of this layer is the average of the NPs height on the surface, extracted from AFM measurements.

The Maxwell-Garnett equation allows calculating the effective refractive index n_{eff} of a matrix with punctual defect. It is important to note that the refractive index and the dielectric constant of a material are linked as follows:

$$\varepsilon_{material} = n_{material}^2 \qquad (1)$$

In this paper, the effective layer is composed by a matrix (dielectric constant: ε_m) of air with NPs defects (dielectric constant: ε_{NP}), with a volumic fraction of NPs in the matrix *f*.

$$\varepsilon_{eff} = \varepsilon_m \frac{2f(\varepsilon_{NP} - \varepsilon_m) + \varepsilon_{NP} + 2\varepsilon_m}{2\varepsilon_m + \varepsilon_{NP} + f(\varepsilon_m - \varepsilon_{NP})} \qquad (2)$$

The volumic fraction of NPs is proportional to the surface coverage of NPs on the gold surface.

The absorption of NPs is taken into account in the complex refractive index of NPs, in Fig. S4 the refractive index is 1.44 + 0.1i ± 0.04. For Fig. S3, the roughness of the surface is taken into account by a modification of the Fresnel coefficient of the layer such as it was done in ref 4.

Fit of the resonance angle of SPR spectra. To fit the resonance angle of experimental SPR spectra (minimum angle) the non-linear least square method coupled with a Monte Carlo random walk was used. First, the refractive range for the Monte Carlo random walk is chosen (in our case, between 1.0 and 2.0). The first step of the algorithm is to select a (random or not) refractive index for the NPs and calculated the associated theoretical SPR curves. Then the least-square error between the experimental SPR minimum spectra and the theoretical ones is calculated. The second step of the algorithm is to use a recursive loop where *N* (*N=1 000 000*, for instance) refractive indexes are selected one by one. For each new refractive index, the theoretical SPR curves have been calculated as well as the least-square error between the experimental SPR minimum spectra and the theoretical ones. When the least-square error from the new refractive index was smaller than the least-square error from the old one, the new refractive index was kept. This simulation has been done several times (1000 for instance) and the refractive index associated with the smallest gives the optimal fit parameter. To calculate the error, the numerical standard deviation has been calculated. The error of the refractive index was calculated using the least-square density of probability (which depends on the standard deviation) and the Metropolis algorithm.

Refractometry. A Bellingham + Stanley RFM-T refractometer was used to extract the refractive index of NPs from the effective refractive index of a NPs/water mixture. Using the volumic fraction and the effective refractive index in the Maxwell-Garnett equation, we were able to work out the refractive index of NPs. The volumic fraction of NPs in water was calculated using the weighting mass of NPs, the water volume and the density of NPs. A refractive index of 1.44 was found for the NPs.

Atomic force microscopy (AFM). AFM images were obtained in ambient conditions using a Nanowizard 4 AFM (JPK Instruments, Germany) equipped with a Vortis SPMControl electronics and an Ultraspeed cantilever holder. Data were collected in Amplitude Modulation AFM mode (AM-AFM mode)[5] using AC160TS cantilevers (Olympus probes, Japan) with nominal resonance frequency ≈ 300 kHz, with scan size of 20 µm X 20 µm (Figure 2 of the main manuscript) and 5 µm X 5 µm (Figure S3) both with 512 x 512 pixels. The cantilever free oscillation amplitude was set to approximately 10 nm and the setpoint amplitude to ≈75 % of it. The scan speed was set to 0.75 – 1 second per line. Data analysis as well as the evaluation of the surface coverage was carried out using Gwyddion Software[6, 7]. Surface coverage was evaluated dividing the total NPs area, evaluated through the definition of a height threshold, by the total area of the full AFM image.

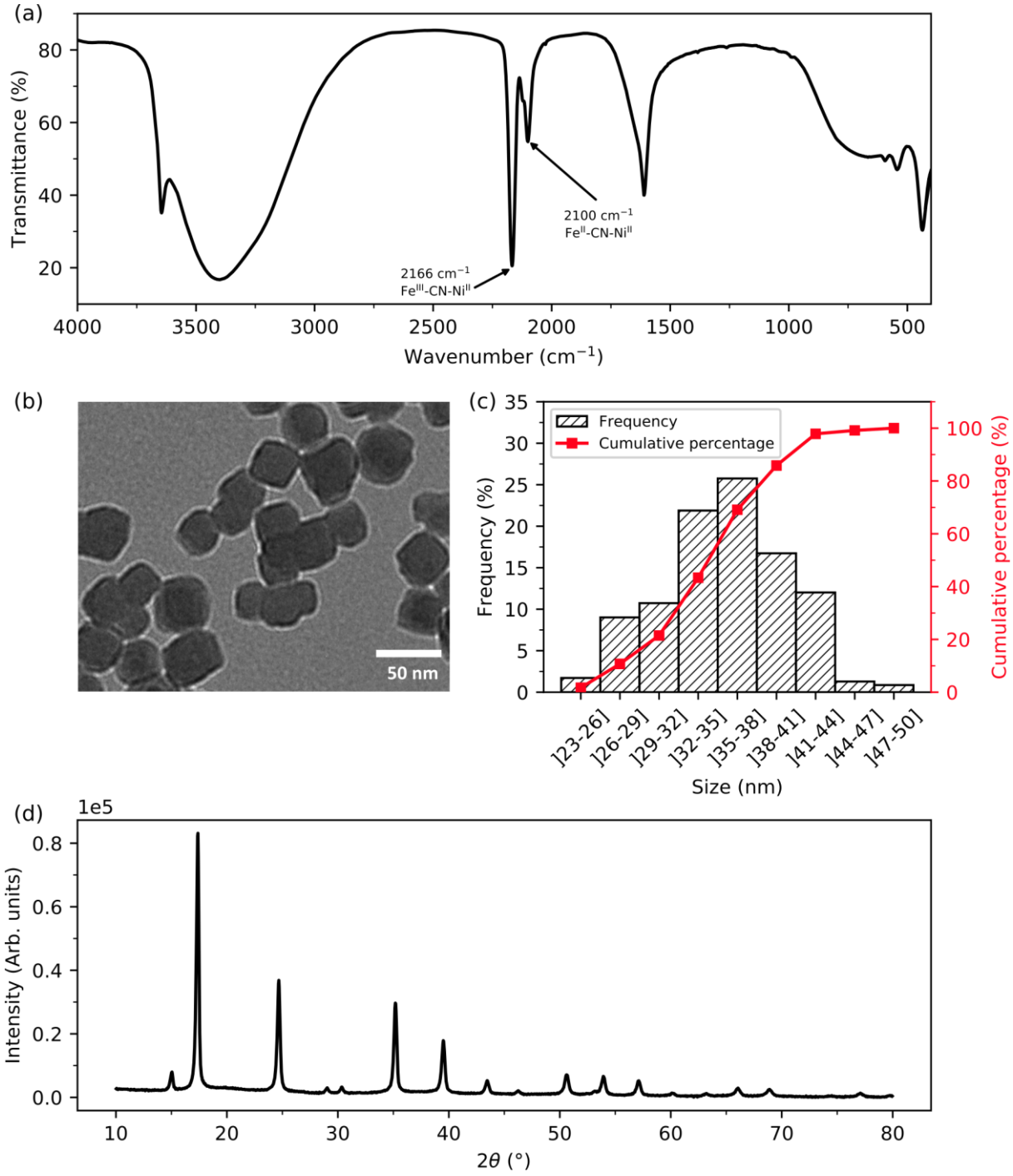

Fig. S1 *Characterization of $K^{+}/Ni^{2+}/[Fe(CN)_6]^{3-}$ PBA NPs (a) Comparaison of infrared spectra between PBA NPs and amino/gold surface, collected by transmission FTIR; (b) TEM image; (c) PBA NPs size distribution determined by TEM measurement; (b) X-Ray diffraction pattern of PBA NPs.*

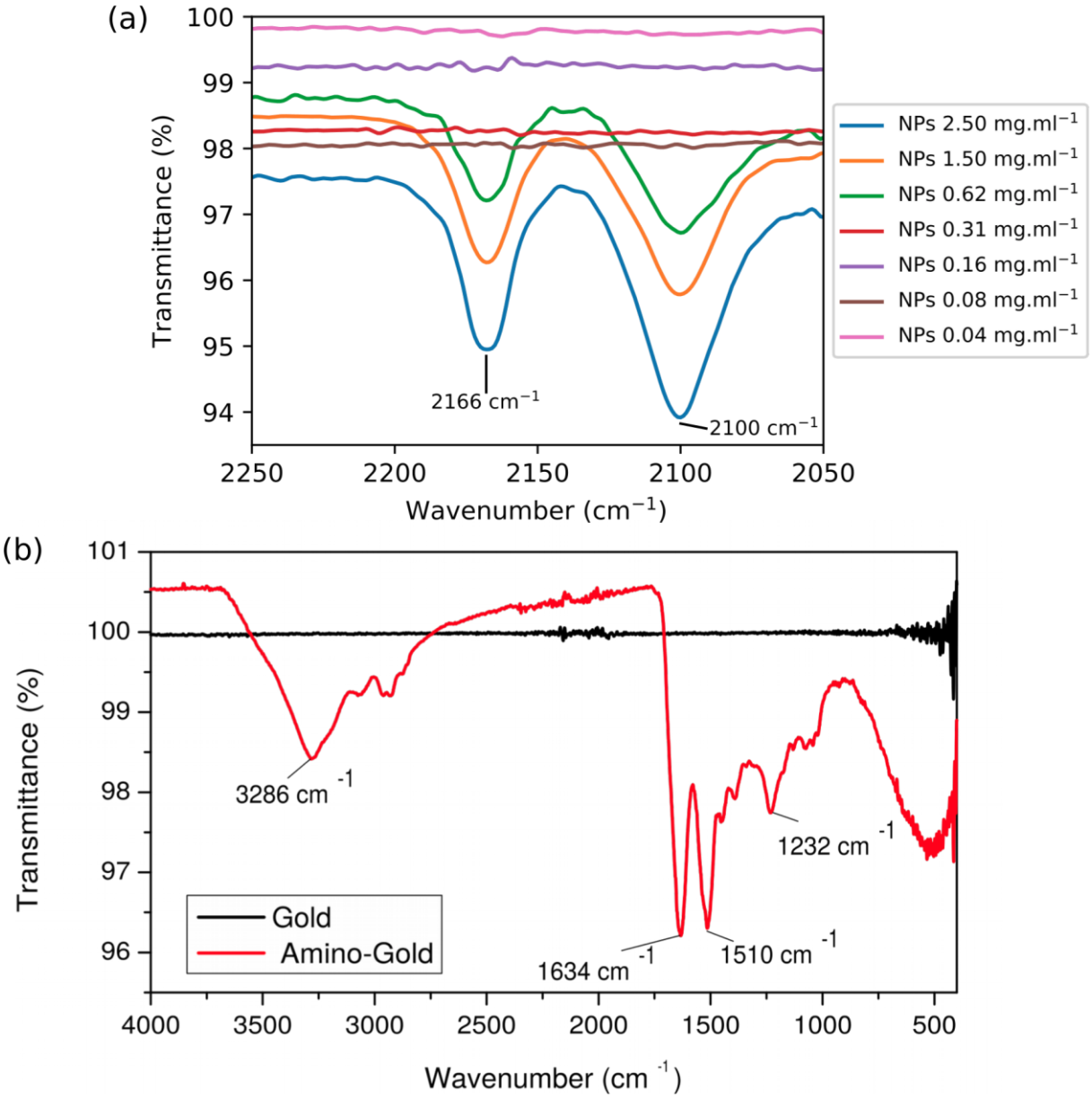

Fig. S2 *(a) Infrared spectra of NPs deposited on amino-gold surface at different concentrations collected by ATR-FTIR (The amino-gold surface was taken as ATR-FTIR reference background); (b) Infrared spectra of gold and amino-gold substrat collected by ATR-FTIR (reference: air).*

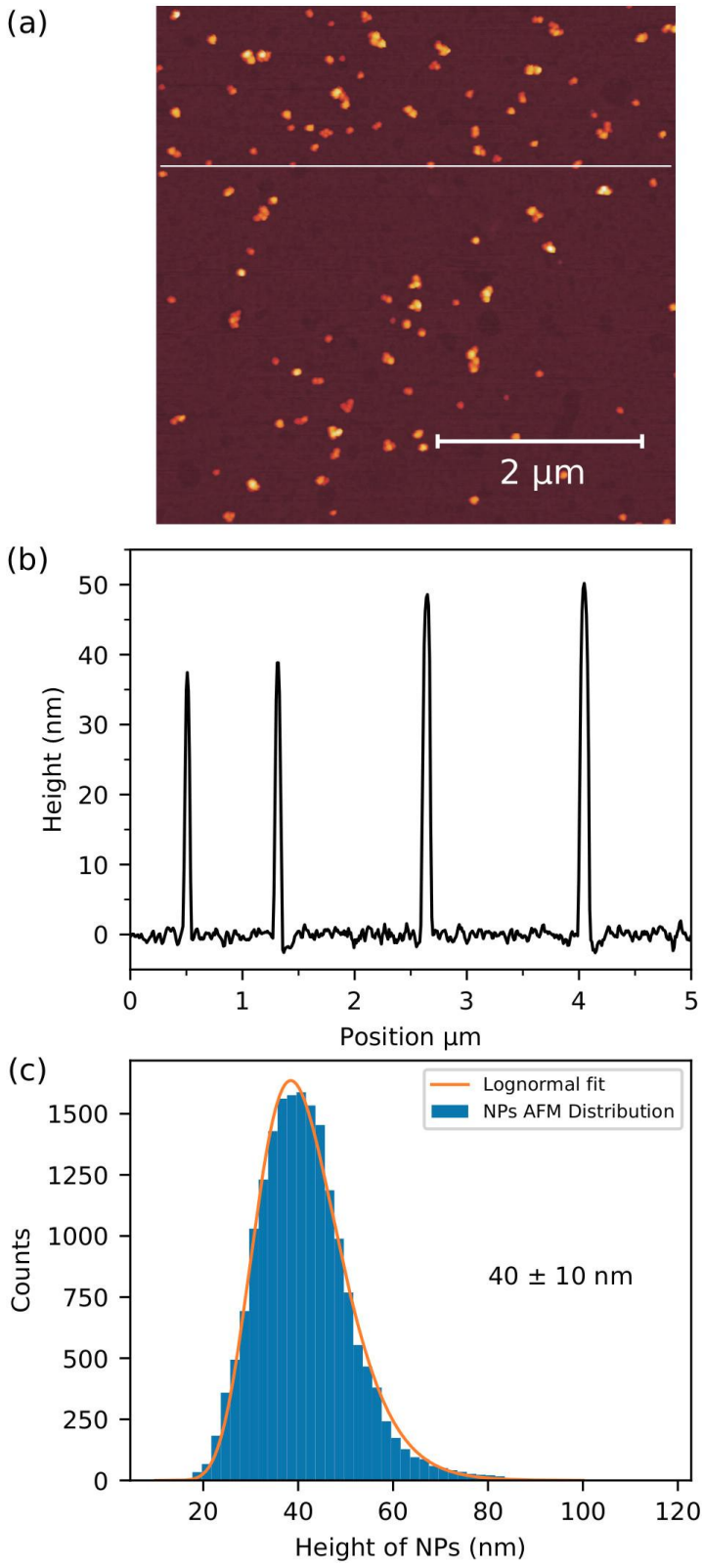

Fig. S3 *AFM Topographical image (scale bar 2 µm) with indicated cross-section (a) and its height profile (b) for NPs deposited on amino-gold surface at 0.16 mg.mL^{-1} concentration; (c) Size distribution of NPs measured with all* topographic AFM image.

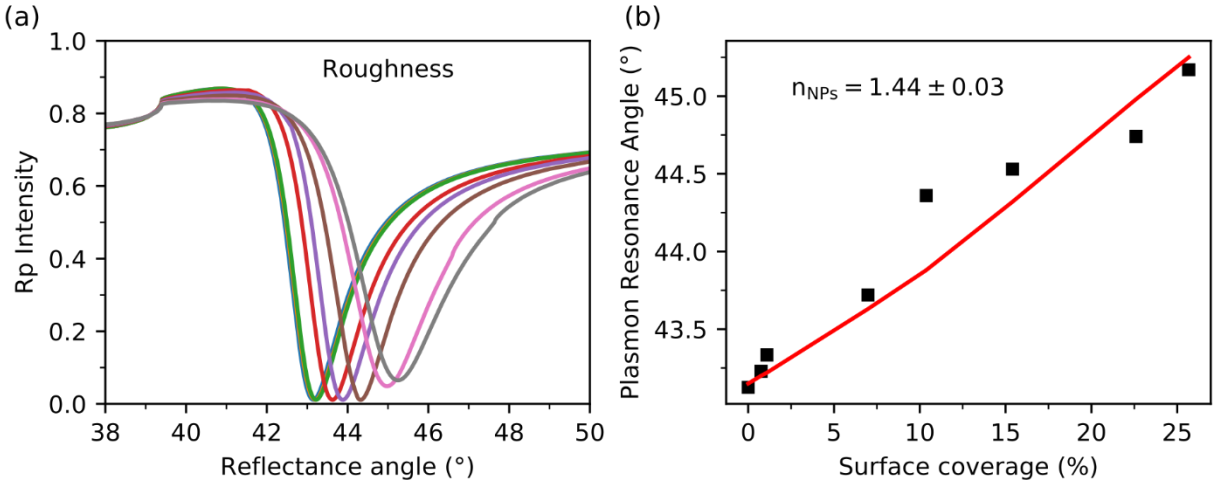

Fig. S4 *(a) Plasmon curves with surface roughness calculated using Rouard method; (b) Plasmon resonance angles represented as a function of the surface coverage of NPs on amino-gold surface.*

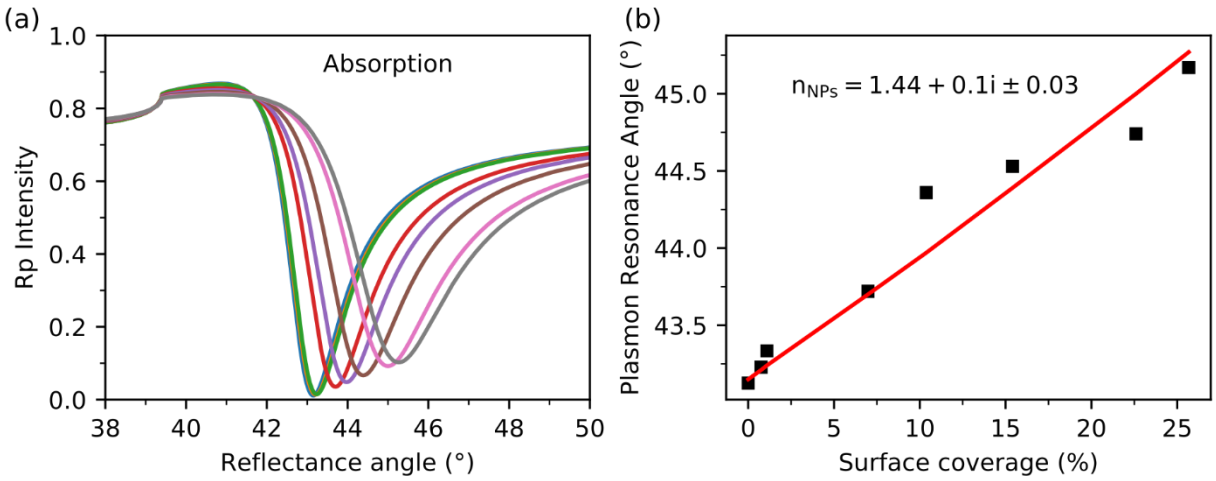

Fig. S5 *(a) Plasmon curves with absorption calculated using Rouard method; (b) Plasmon resonance angles represented as a function of the surface coverage of NPs on amino-gold surface.*

The CBS is a member of the France-BioImaging (FBI) and the French Infrastructure for Integrated Structural Biology (FRISBI), 2 national infrastructures supported by the French National Research Agency (ANR-10-INBS-04-01 and ANR-10-INBS-05, respectively). Oscar Saavedra acknowledges funding from the European Union's Horizon 2020 research and innovation program under the Marie Sklodowska-Curie grant agreement No. 721874 (SPM2.0).

1. G. Félix, W. Nicolazzi, L. Salmon, G. Molnár, M. Perrier, G. Maurin, J. Larionova, J. Long, Y. Guari and A. Bousseksou, *Phys. Rev. Lett.*, 2013, **110**, 235701.
2. G. Maurin-Pasturel, E. Rascol, M. Busson, S. Sevestre, J. Lai-Kee-Him, P. Bron, J. Long, J. Chopineau, J.-M. Devoisselle, Y. Guari and J. Larionova, *Inorg. Chem. Front.*, 2017, **4**, 1737-1741.
3. C. Rossi, J. Homand, H. Hamdi, C. Bauche, D. Ladant and J. Chopineau, *Biochemistry*, 2003, **42**, 15273-15283.
4. G. Lérondel and R. Romestain, *Applied Physics Letters*, 1999, **74**, 2740-2742.
5. R. García, *Amplitude Modulation Atomic Force Microscopy: GARCIA:AMPLIT.MODULATION O-BK*, Wiley-VCH Verlag GmbH & Co. KGaA, Weinheim, Germany, 2010.
6. D. Nečas and P. Klapetek, *Open Physics*, 2011, **10**, 181-188.
7. A. Theodoratou, L. Costa, L. Bonnet, C. Blanc, V. Lapinte, P. Etienne, P.-E. Milhiet, J.-J. Robin, J. Oberdisse, J. Chopineau and A. Aubert-Pouëssel, *European Polymer Journal*, 2019, **111**, 161-169.